11th International Symposium on Turbulence and Shear Flow Phenomena (TSFP11)
Southampton, UK, July 30 to August 2, 2019

INTERNAL LAYERS OF INTENSE SHEAR IN A MIXING LAYER AT HIGH REYNOLDS NUMBER

Daniele Fiscaletti
Department of Aerospace Engineering,
University of Bristol,
Bristol BS8 1TR, United Kingdom,
d.fiscaletti@bristol.ac.uk

Antonio Attili
Institute for Combustion Technology,
RWTH Aachen University,
52056 Aachen, Germany,
a.attili@itv.rwth-aachen.de

INTRODUCTION

The characteristics of layers of intense shear are investigated in the fully-developed turbulent region of a mixing layer at high Reynolds number. The database employed has been generated with a large scale Direct Numerical Simulation (DNS).

In the last few decades, numerical and experimental investigations showed that a thin layer separates the turbulent region from the non-turbulent irrotational fluid in a number of different flow configurations. At this thin layer, commonly known as turbulent/non-turbulent interface (TNTI), a jump in velocity, vorticity, and concentration of passive scalar was observed and quantified (see da Silva *et al.* (2014)). This jump was found to govern the entrainment and the growth rate of the turbulent flow.

Recently, Eisma *et al.* (2015) showed that layers of intense shear, somehow similar to the TNTI, exist within the internal region of a turbulent boundary layer. Later, de Silva *et al.* (2017) examined the interfaces between adjacent uniform momentum zones in a turbulent boundary layer. Both studies showed that jumps in the streamwise velocity exist across internal layers, and scale with the friction velocity, while the thickness of these interfaces scales with the Taylor microscale. Layers of intense shear were also reported in homogeneous isotropic turbulence at very high Reynolds number, both from statistical considerations (Elsinga *et al.* (2017)) and instantaneous snapshots (Ishihara *et al.* (2013)). The analysis of the average flow pattern in the local coordinate system defined by the eigenvectors of the strain rate tensor revealed a shear-layer structure consisting of aligned vortical motions (Elsinga & Marusic (2010), Elsinga *et al.* (2017)). A similar structure was also observed from instantaneous snapshots, where sharp layers of approximately four Taylor length scales of thickness were found to bound regions of different large-scale velocities (Ishihara *et al.* (2013)).

The existence of internal layers was so far ascertained in turbulent boundary layers and in homogeneous isotropic turbulence, while boundary-free shear flows have never been examined. Moreover, while Attili *et al.* (2014) and Gampert *et al.* (2014) reported a jump across the TNTI of a mixing layer, the concentration of a passive scalar across the internal layers has never been analysed.

The main goal of the present study is to investigate the internal layers of a mixing layer at high Reynolds number. Profiles of velocity and scalar concentration at different Schmidt numbers are examined across these layers. Three different streamwise locations, characterised by different Reynolds number, are considered. The largest Reynolds number of the mixing layer under analysis is $Re_\lambda = 275$, and to the authors' best knowledge, this is the largest ever achieved in DNS simulations of this flow.

NUMERICAL SIMULATIONS

The dataset employed in the present analysis was generated with a large-scale DNS of a high Reynolds number, spatially developing, mixing layer, featuring a grid of about 18×10^9 points. The configuration and methods applied in these simulations are described in details by Attili & Bisetti (2012) and Attili *et al.* (2014). Analogous DNS datasets of a mixing layer were previously employed to investigate the interaction between the large and the small scales of turbulence (Fiscaletti *et al.* (2016*b*) and Fiscaletti *et al.* (2016*a*)). Compared to the simulations described in the cited papers, the Reynolds number of the turbulent flow that is analysed here was increased up to $Re_\lambda \approx 275$.

METHOD OF ANALYSIS

A Cartesian system of coordinates is introduced within the numerical dataset, where the x-axis is oriented along the streamwise direction of the flow, the y-axis along the crosswise direction, and the z-axis along the spanwise direction. The coordinate system is centred in a corner of the three-dimensional numerical domain, on the low velocity side. The method for the identification of the internal layers, and for the calculation of the conditional averages of velocities and scalar concentration is presented in this Section.

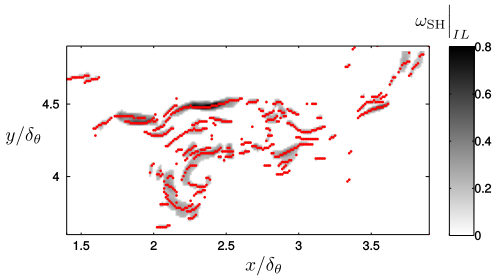

Figure 1. Shapshot of $\omega_{SH}(x,y,z)\big|_{IL}$ at constant z, obtained as explained in Equation 2. Streamwise and crosswise coordinates, respectively x and y, are non-dimensionalized by the local momentum thickness δ_θ. The red dots are the local maxima of $\omega_{SH}(x,y,z)\big|_{IL}$ along the crosswise direction y, and indicate points of internal layers.

1. With the aim of detecting the internal layers, we apply the triple decomposition method introduced by Kolář (2007). The velocity gradient tensor is decomposed into the sum of three different terms, which account for rigid-body rotation, elongation, and shear:

$$\nabla \mathbf{u} = (\nabla \mathbf{u})_{RR} + (\nabla \mathbf{u})_{EL} + (\nabla \mathbf{u})_{SH} \qquad (1)$$

   Among these three terms, only the shear contribution was considered in the calculation of the vorticity, $\omega_{SH}(x,y,z)$. An analogous approach was applied by Eisma *et al.* (2015), and further details can be found in their paper.
2. The mean of the shear component of the vorticity is calculated, $\overline{\omega_{SH}}(x,y)$, in the entire domain.
3. At each streamwise location, the maximum of $\overline{\omega_{SH}}(x,y)$ is calculated and the following threshold is applied to identify the internal layers *IL*:

$$\omega_{SH}(x,y,z)\Big|_{IL} > K \cdot \overline{\omega_{SH}}^{max,y}(x) \qquad (2)$$

   where K is a constant. The value of K is chosen in such a way to identify only the intense events and, at the same time, to identify a sufficiently large statistical sample to guarantee statistical convergence. In the present analysis, $K = 1.5$. In points where the condition expressed in Equation 2 is not verified, $\omega_{SH}(x,y,z)\big|_{IL}$ is set to be equal to zero. A snapshot of $\omega_{SH}(x,y,z)\big|_{IL}$ is given in figure 1.
4. Inside the zones where the condition given in Equation 2 is verified, the local maxima along the crosswise direction are calculated, at each downstream location. These maxima are considered points of the internal layers (red dots in figure 1).
5. The TNTI, the interface separating the turbulent region from the irrotational external fluid, is detected using a threshold on the vorticity magnitude, which is determined following the method proposed by Taveira & da Silva (2013), and summarized in the Appendix 1 of Attili *et al.* (2014). In figure 2, a snapshot of the magnitude of $\nabla c(x,y,z)$ is presented, where c is a passive scalar with Schmidt number $Sc = 1.4$. The turbulent region is bounded by the TNTI, which is evidenced by the black continuous line.

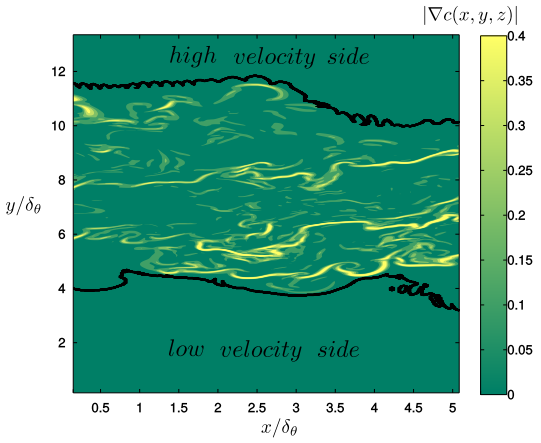

Figure 2. Magnitude of $\nabla c(x,y,z)$ on a plane at constant z, in a streamwise region where $Re_\lambda \approx 250$. The streamwise and crosswise coordinates, respectively x and y, are non-dimensionalized by an averaged momentum thickness δ_θ in this region. The black lines indicate the turbulent/non-turbulent interfaces on both the high and the low velocity side of the mixing layer.

6. Profiles centred in the points obtained as explained the step 4 are computed along the crosswise direction. Only samples located inside the TNTI are retained, and contribute to statistics.
7. These profiles are averaged conditioned on the streamwise velocity u_i of the points of $\omega_{SH}(x,y,z)\big|_{IL}$ where $\omega_{SH}(x,y,z)$ is maximum along y (red dots in figure 1). In particular, the conditional averages of the velocity profiles are calculated depending on the velocity range $(\Delta U - u_i)/u_{rms}$ to which u_i belongs.

RESULTS AND DISCUSSION

Figure 3 shows conditionally-averaged profiles of the streamwise velocity across the internal layers of intense shear, obtained as discussed in the previous section, at two different downstream locations in the mixing layer, cor-

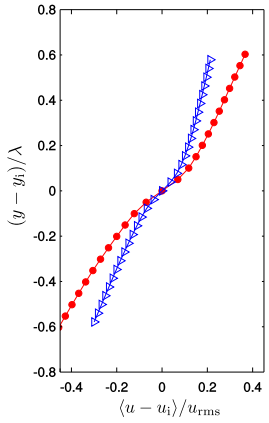

Figure 3. Conditionally-averaged profiles of the streamwise velocity in the near-vicinity of all detected internal layers within the range $0.25 < (\Delta U - u_i)/u_{rms} < 0.50$. Red full • symbols are obtained at $Re_\lambda \approx 200$, blue empty ▷ at $Re_\lambda \approx 275$.

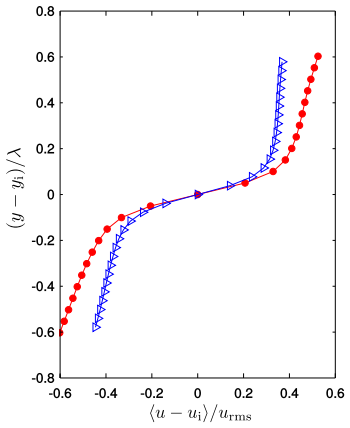

Figure 4. As in figure 3, but only *positive* gradients of $\left.\frac{du}{dy}\right|_{IL}$ at all detected internal layers were retained and contributed to the conditionally-averaged profiles of streamwise velocity.

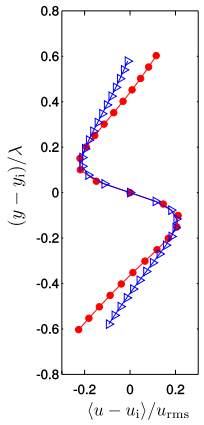

Figure 5. As in figure 3, but only *negative* gradients of $\left.\frac{du}{dy}\right|_{IL}$ at all detected internal layers are retained and contributed to the conditionally-averaged profiles of streamwise velocity.

responding to Reynolds number based on the Taylor microscale of $Re_\lambda \approx 200$ and $Re_\lambda \approx 275$. All detected internal layers used to compute the velocity profiles in figure 3 are characterised by $0.25 < (\Delta U - u_{\rm i})/u_{\rm rms} < 0.50$, where ΔU is the difference in streamwise velocity between the high velocity side and the low velocity side of the mixing layer. Velocity jumps of modest intensity can be observed to occur across the internal layers of intense shear. Analogous velocity jumps were found at different ranges of non-dimensional velocities $(\Delta U - u_{\rm i})/u_{\rm rms}$ (not shown). These velocity jumps can be quantified by applying a fitting to the linear branches of the conditional profiles, as in figure 7(b) of de Silva *et al.* (2017). According to this quantification, the non-dimensional velocity jumps $(\delta u/u_{\rm rms})$ can be estimated to be of 0.17 and 0.11, respectively for $Re_\lambda \approx 200$ and 275. This is one order of magnitude lower than the velocity jump observed by Ishihara *et al.* (2013) in homogeneous isotropic turbulence, which was however quantified from instantaneous snapshots of the intense shear layers.

The conditional velocity profiles presented in figure 3 do not distinguish between positive or negative crosswise gradients of the streamwise velocity $\left.\frac{du}{dy}\right|_{IL}$. If we consider only the velocity profiles characterised by *positive* $\left.\frac{du}{dy}\right|_{IL}$ at the internal layers, different conditionally-averaged profiles are obtained (figure 4). Velocity jumps of much larger intensity, of the order of magnitude of $u_{\rm rms}$, can be observed in this case. Jumps of comparable intensity are also observed when retaining only those velocity profiles characterised by *negative* $\left.\frac{du}{dy}\right|_{IL}$ at the internal layers, as showed in figure 5. The percentage of profiles with $\left.\frac{du}{dy}\right|_{IL} > 0$ over the total profiles is found to range between 60% and 70%, depending on the crosswise position within the flow, the non-dimensional velocity $(\Delta U - u_{\rm i})/u_{\rm rms}$), and the Reynolds number. Therefore, profiles with $\left.\frac{du}{dy}\right|_{IL} > 0$ are dominant, which explains the similar trends observed in figures 3 and 4. A non-negligible percentage of velocity profiles at the internal layers (between 30 and 40%) is characterised by *negative* $\left.\frac{du}{dy}\right|_{IL}$, which leads to mild velocity jumps when all the detected internal layers are considered in the computation of the conditionally-averaged profiles (figure 3).

The velocity jumps of the internal layers at the three different Reynolds number and at the different ranges of non-dimensional velocities $(\Delta U - u_{\rm i})/u_{\rm rms}$ are presented in figure 6. Specifically, figure 6a and 6c report the strength of the velocity jumps associated with profiles where $\left.\frac{du}{dy}\right|_{IL} > 0$, while in figure 6b and 6d the velocity jumps are associated with profiles where $\left.\frac{du}{dy}\right|_{IL} < 0$. In the top figures, the velocity jumps are non-dimensionalized by the *rms* velocity, while in the bottom figures the non-dimensionalization is done by the large-scale quantity ΔU, the velocity difference across the mixing layer.

As it can be observed in figure 6, velocity jumps of more than 10% of ΔU are found on a statistical sense across the identified layers of intense shear. Also, δu appears

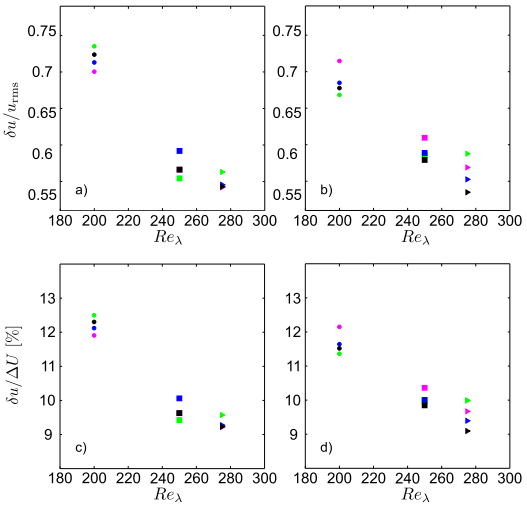

Figure 6. Velocity jump at the internal layers identified by setting $K = 1.5$ in Equation 2 for (*a,c*) *positive* and (*b,d*) *negative* values of $\left.\frac{du}{dy}\right|_{IL}$ detected within the ranges (green symbols) $-0.25 < (\Delta U - u_{\rm i})/u_{\rm rms} < 0$, (magenta) $0 < (\Delta U - u_{\rm i})/u_{\rm rms} < 0.25$, (blue) $0.25 < (\Delta U - u_{\rm i})/u_{\rm rms} < 0.50$, and (black) $0.50 < (\Delta U - u_{\rm i})/u_{\rm rms} < 0.75$. • indicate $Re_\lambda \approx 200$, ■ $Re_\lambda \approx 250$, ► $Re_\lambda \approx 275$.

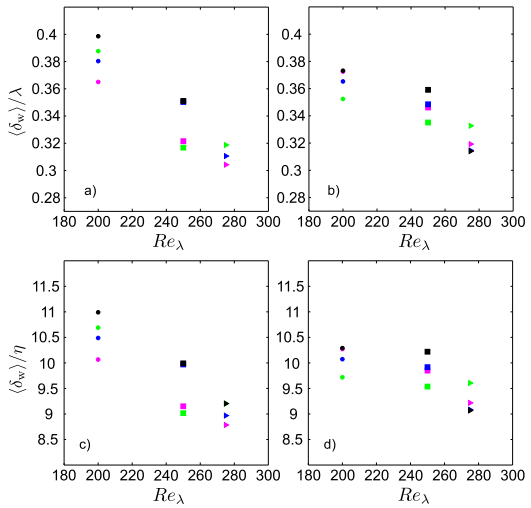

Figure 7. Thickness of the internal layers identified by setting $K = 1.5$ in Equation 2 for (*a,c*) *positive* and (*b,d*) *negative* values of $\frac{du}{dy}\Big|_{IL}$ detected within the ranges (green symbols) $-0.25 < (\Delta U - u_i)/u_{rms} < 0$, (magenta) $0 < (\Delta U - u_i)/u_{rms} < 0.25$, (blue) $0.25 < (\Delta U - u_i)/u_{rms} < 0.50$, and (black) $0.50 < (\Delta U - u_i)/u_{rms} < 0.75$. • refer to $Re_\lambda \approx 200$, ■ to $Re_\lambda \approx 250$, ▶ to $Re_\lambda \approx 275$.

to not depend on the range of non-dimensional velocities where these intense shear layers are detected. This is different from what was found in a turbulent boundary layer, where larger velocity jumps were detected closer to the wall, therefore at increasingly larger momentum deficits (Eisma *et al.* (2015), de Silva *et al.* (2017)). It can also be observed that these velocity jumps non-dimensionalized by the constant quantity ΔU are characterised by decreasing intensities for growing Re_λ, both for positive and negative gradients of $\frac{du}{dy}\Big|_{IL}$ (figure 6c and 6d).

The velocity jumps across intense shear layers that are quantified in the present mixing layer can be compared with those found in different turbulent flows. From DNS simulations of homogeneous isoentropic turbulence at very large Re_λ, Ishihara *et al.* (2013) examined instantaneous snapshots of extreme shear events. The authors reported velocity jumps of the order of the velocity *rms*, which is consistent with the finding of the present analysis (figure 6). From their analysis on DNS data of both a channel flow and a turbulent boundary layer, Wei *et al.* (2014) reported velocity jumps of approximately half the *rms* velocity (their figure 6d). Similar to Wei *et al.* (2014), de Silva *et al.* (2017) and Eisma *et al.* (2015) reported smaller velocity jumps than those obtained here from their experimental investigations on turbulent boundary layers (see figure 13b of de Silva *et al.* (2017) and figure 8a of Eisma *et al.* (2015)).

Following Brown & Roshko (1974), the thickness of the internal layers of intense shear δ_w can be estimated as the ratio between the velocity jump δu and the maximum local gradient of the profile $\partial\langle u - u_i\rangle/\partial y\Big|_{max}$. The thickness of the internal layers associated with profiles with $\frac{du}{dy}\Big|_{IL} > 0$ and with $\frac{du}{dy}\Big|_{IL} < 0$ is presented respectively in figures 7a and 7c, and in figures 7b and 7d. This thickness is non-dimensionalized by the Taylor microscale λ (figures 7a and 7b) and by the Kolmogorov microscale η (figures 7c and 7d), and estimated at different Re_λ, i.e. different streamwise locations, and at different ranges of streamwise velocities $(\Delta U - u_i)/u_{rms}$.

From figure 7, it is not possible to establish whether the thickness of the internal layers scales with the Taylor lenght scale or with the Kolmogorov length scale. This is because the range of Reynolds number under analysis is not sufficiently large. However, several important observations can be made. Firstly, the thickness of the internal layers seems to be insensitive to the velocity range $(\Delta U - u_i)/u_{rms}$. Secondly, δ_w/λ ranges between 0.3 and 0.4, which is the same as what found by Eisma *et al.* (2015) (their figure 8b), and very similar to what found by de Silva *et al.* (2017) (their figure 13e) in turbulent boundary layers. Moreover, δ_w/η is nearly equal to 10, which is the characteristic diameter of the small-scale coherent structures according to several studies including Ishihara *et al.* (2013) and Fiscaletti *et al.* (2014), the so-called *worms*. It can also be observed that δ_w remains nearly constant over the four ranges of streamwise velocities under analysis, and it shows a decrease when moving from $Re_\lambda \approx 200$ to $Re_\lambda \approx 275$. This is analogous to what observed for the velocity jump δu.

After having examined the profiles of streamwise velocity across the internal layers of intense shear, and having quantified both their velocity jump and their thickness, we look at the scalar concentration across these internal layers. In figure 8, we present conditionally-averaged profiles of scalar concentration at Schmidt number $Sc = 1.4$ in the near-vicinity of all detected internal layers, within the range $0.25 < (\Delta U - u_i)/u_{rms} < 0.50$, at $Re_\lambda \approx 200$ and 275. The profiles of the scalar concentration are nearly insensitive to the presence of internal layers of intense shear. A completely different behaviour can be observed here when compared with the conditional averages of scalar concentration across the TNTI reported by Attili *et al.* (2014) and Gampert *et al.* (2014), who showed remarkably large jumps of the scalar concentration at the TNTI.

A first important conclusion is that regions of intense shear are not characterised by strong gradients of a passive scalar. Therefore, these internal layers, which bound regions of different momentum, do not seem to bound regions of different passive scalar according to our finding from figure 8. It is worth pointing out that this finding is independent of the method that is adopted for the identification of

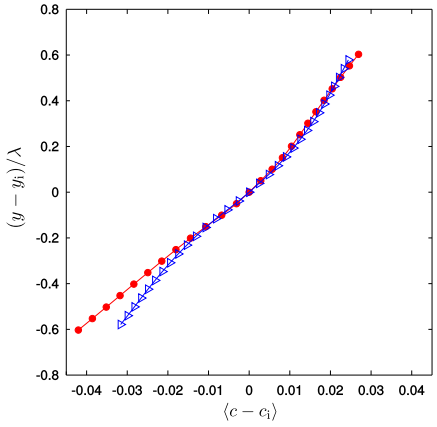

Figure 8. Conditionally-averaged profiles of scalar concentration at Schmidt number $Sc = 1.4$ in the near-vicinity of all detected internal layers within the range $0.25 < (\Delta U - u_i)/u_{rms} < 0.50$. Symbols are defined in figure 2.

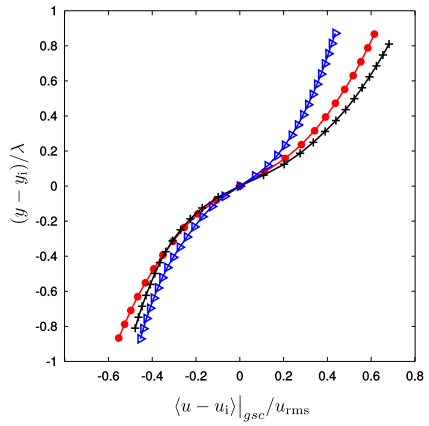

Figure 9. Conditionally-averaged profiles of streamwise velocity in the near-vicinity of points of intense magnitude of the scalar gradient $|\nabla c(x,y,z)|$, within the range $0.25 < (\Delta U - u_i)/u_{\rm rms} < 0.50$. Red full • indicate $Re_\lambda \approx 200$, black + $Re_\lambda \approx 250$, blue empty ▷ $Re_\lambda \approx 275$.

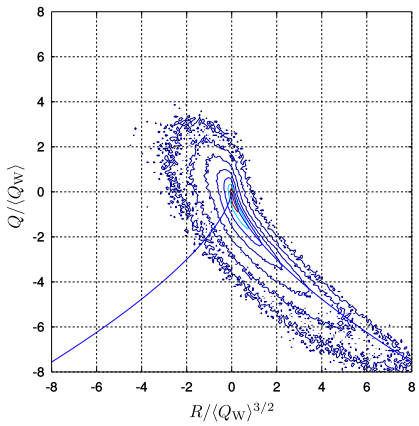

Figure 10. Joint probability density function of the second (Q) and third (R) invariants of the velocity gradient tensor in points of the flow domain characterised by intense magnitude of $|\nabla c(x,y,z)|$, at $Re_\lambda \approx 275$.

these internal layers. A method analogous to the one described in de Silva *et al.* (2017) is also applied, with the aim of identifying the internal layers. This method is based on the local probability density function for the identification of the edges of the uniform momentum zones. Even if additional details on this analysis are not reported here for the sake of brevity, conditionally-averaged profiles analogous to those presented in figure 8 are obtained.

If we look at the spatial organization of a passive scalar, this seems to be arranged into layers that preferentially develop along the streamwise direction, x. The described organization of the passive scalar into streamwise layers can be observed in figure 2. From this observation, it can be of interest to check whether strong scalar gradients can be associated with jumps of the streamwise velocity. The analysis has the aim of determining whether, across these layers, the crosswise profiles of both momentum and passive scalar exhibit analogous behaviours. After identifying points characterised by an intense magnitude of the scalar gradient $|\nabla c(x,y,z)|$, we thus calculate the profiles of the conditional average of the streamwise velocity around these points. This conditional averaging is identified by the subscript *gsc*. The results are presented in figure 9. As it can be observed, the profiles of streamwise velocity are characterised by a jump, which seems to be stronger for decreasing Reynolds number. The conditionally-averaged profiles presented in figure 9 include all the points of intense magnitude of the scalar gradient $|\nabla c(x,y,z)|$. However, analogous to what we have previously done for the velocity profiles across the internal layers, these profiles can also be conditioned on the sign of the crosswise gradient of the streamwise velocity $\left.\frac{du}{dy}\right|_{gsc}$ (see figures 4 and 5). Although the results of this additional conditioning are not reported here, a much larger velocity jump exists when conditioning these averages on the positive gradients of $\left.\frac{du}{dy}\right|_{gsc}$, whereas a profile similar to the one reported in figure 5 is obtained when the conditioning is on the negative gradients of $\left.\frac{du}{dy}\right|_{gsc}$.

From this analysis, it can be observed that in certain regions of the flow domain characterised by a strong magnitude of the scalar gradient, $|\nabla c(x,y,z)|$, both the streamwise velocity and the passive scalar show a jump along the crosswise direction y, i.e. along the direction of mean shear. These regions are shaped as layers elongated along the x direction, as it can be seen in figure 2. The simultaneous presence of a jump across these layers both in the streamwise velocity and in the passive scalar suggests that analogies could exist between these layers and the TNTI. With the aim of exploring the existence of additional similarities between the layers of intense $|\nabla c(x,y,z)|$ and the TNTI, the flow topology of the points constituting these layers is examined.

The flow topology can be investigated by looking at the joint probability density function of the second and third invariants of the velocity gradient tensor, Q and R, respectively, as explained in Chong *et al.* (1990). The results of this analysis are reported in figure 10. As it can be observed, two flow topologies are mainly present in these layers of intense $|\nabla c(x,y,z)|$. Following Chong *et al.* (1990), these are the unstable node/saddle/saddle and the stable focus/stretching. The strong prevalence of the unstable node/saddle/saddle is an evidence that the flow is strain-dominated. These observations are consistent with Brethouwer *et al.* (2003) and Elsinga & da Silva (2019), among others. The jpdf of conditional Q and R presented in figure 10 deviates significantly from the unconditional jpdf,

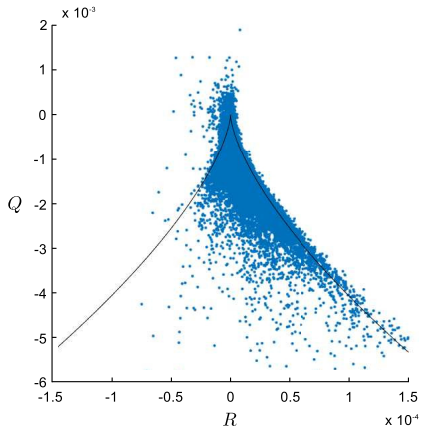

Figure 11. QR scatter plot at $y_{\rm I} = 6\eta$ from the TNTI inside the turbulent region, at $Re_\lambda \approx 250$.

which, even if it is not reported here, has the characteristic teardrop shape, regarded as a universal characteristic of the small-scale turbulence (Elsinga & Marusic (2010)).

The second and third invariants of the velocity gradient tensor are also calculated in the proximity to the TNTI, specifically in points located at a crosswise distance of 6η with respect to the TNTI, inside the turbulent region. The scatter plot of these invariants is presented in figure 11. Similar to the jpdf given in figure 10, a prevalence of unstable node/saddle/saddle flow topology is found, which is again evidence that strain dominates over vorticity. Therefore, we can conclude that both the internal side of the TNTI and the layers of intense $|\nabla c(x,y,z)|$ are characterised by analogous strain-dominated topological contents.

CONCLUSION

In this work, the properties of the internal layers of intense shear were investigated in a mixing layer, at high Reynolds number. These internal layers were identified with a criterion based on the large values of the shear vorticity. In particular, after decomposing the velocity gradient tensor into three contributors, i.e. elongation, rigid-body rotation, and shear, only the shear component was used for the calculation of the vorticity. Conditionally-averaged profiles of the streamwise velocity and of a passive scalar with $Sc = 1.4$ were calculated across these layers. The velocity profiles were also conditioned on the sign of the crosswise gradients $\frac{du}{dy}$ at the layers.

The results show jumps in the streamwise velocity of around 10% ΔU, where ΔU is the difference in the streamwise velocity between the high velocity side and the low velocity side of the mixing layer. This is considerably larger than what de Silva *et al.* (2017) and Eisma *et al.* (2015) found in turbulent boundary layers. From these velocity profiles, the characteristic thickness of the internal layers could be estimated. When non-dimensionalised by the Taylor length scale λ, this thickness was observed to range between 0.3 and 0.4 λ, while a thickness of approximately 10η was found, where the non-dimensionalization was by η, the Kolmogorov length scale. On the other hand, the profiles of a passive scalar across the internal layers did not exhibit any jumps. This indicates that the concentration of a passive scalar changes nearly-uniformly across the layers of intense shear vorticity. Therefore, these internal layers, which bound regions of different momentum, do not appear to bound regions of different passive scalar.

Later, we focused on the layers of intense magnitude of the scalar gradient $|\nabla c(x,y,z)|$, which, similar to the shear layers, appear elongated along the streamwise direction of the flow (figure 2). Across these layers, conditionally-averaged profiles of the streamwise velocity were calculated. It was found that the profiles are characterised by a clear jump. As a consequence, layers of intense scalar gradients appear to separate both regions of different passive scalar and regions of different momentum. This observation suggested that an important analogy exists between these layers and the internal side of the TNTI, which was later confirmed by examining the second and third invariants of the velocity gradient tensor in these points. A prevalence of unstable node/saddle/saddle flow topology was found in both layers, which is evidence of strain-dominated features.

REFERENCES

Attili, A. & Bisetti, F. 2012 Statistics and scaling of turbulence in a spatially developing mixing layer at $re_\lambda = 250$. *Phys. Fluids* **24**, 035109.

Attili, A., Cristancho, J.C. & Bisetti, F. 2014 Statistics of the turbulent/non-turbulent interface in a spatially developing mixing layer. *J. Turbul.* **15** (9), 555–568.

Brethouwer, G., Hunt, J.C.R. & Nieuwstadt, F.T.M 2003 Micro-structure and lagrangian statistics of the scalar field with a mean gradient in isotropic turbulence. *J. Fluid Mech.* **474**, 193–225.

Brown, G.L. & Roshko, A. 1974 On density effects and large structure in turbulent mixing layers. *J. Fluid Mech.* **64** (4), 775–816.

Chong, M.S., Perry, A.E. & Cantwell, B.J. 1990 A general classification of threedimensional flow fields. *Phys. Fluids A* **2**, 765–777.

Eisma, J., Westerweel, J., Ooms, G. & Elsinga, G.E. 2015 Interfaces and internal layers in a turbulent boundary layer. *Phys. Fluids* **27** (5), 055103.

Elsinga, G.E., Ishihara, T., Goudar, M.V. & da Silva, C.B. 2017 The scaling of straining motions in homogeneous isotropic turbulence. *J. Fluid Mech.* **829**, 31–64.

Elsinga, G.E. & Marusic, I. 2010 Universal aspects of small-scale motions in turbulence. *J. Fluid Mech.* **662**, 514–539.

Elsinga, G.E. & da Silva, C.B. 2019 How the turbulent/non-turbulent interface is different from internal turbulence. *J. Fluid Mech.* **866**, 216–238.

Fiscaletti, D., Attili, A., Bisetti, F. & Elsinga, G.E. 2016*a* Scale interactions in a mixing layer – the role of the large-scale gradients. *J. Fluid Mech.* **791**, 154–173.

Fiscaletti, D., Elsinga, G.E., Attili, A., Bisetti, F. & Buxton, O.R.H. 2016*b* Scale dependence of the alignment between strain rate and rotation in turbulent shear flow. *Phys. Rev. Fluids* **1**, 064405.

Fiscaletti, D., Westerweel, J. & Elsinga, G.E. 2014 Long-range μpiv to resolve the small scales in a jet at high reynolds number. *Exp. Fluids* **55**, 1812.

Gampert, M., Boschung, J., Hennig, F., Gauding, M & Peters, N. 2014 The vorticity versus the scalar criterion for the detection of the turbulent/non-turbulent interface. *J. Fluid Mech.* **750**, 578–596.

Ishihara, T., Kaneda, Y. & Hunt, J.C.R. 2013 Thin shear layers in high reynolds number turbulence - dns results. *Flow Turb. Comb.* **91**, 895–929.

Kolář, V. 2007 Vortex identification: New requirements and limitations. *Int. J. Heat Fluid Flow* **28**, 638–652.

da Silva, C.B., Hunt, J.C.R., Eames, I. & Westerweel, J. 2014 Interfacial layers between regions of different turbulence intensity. *Annu. Rev. Fluid Mech.* **46**, 567–590.

de Silva, C.M., Philip, J., Hutchins, N. & Marusic, I. 2017 Interfaces of uniform momentum zones in turbulent boundary layers. *J. Fluid Mech.* **820**, 451–478.

Taveira, R. & da Silva, C.B. 2013 Kinetic energy budgets near the turbulent/nonturbulent interface in jets. *Phys. Fluids* **25**, 015114.

Wei, L., Elsinga, G.E., Brethouwer, G., Schlatter, P. & A.V., Johansson 2014 Universality and scaling phenomenology of small-scale turbulence in wall-bounded flows. *Phys. Fluids* **26**, 035107.